

Helsinki University of Technology  
Low Temperature Laboratory  
Espoo 2005

# **JOSEPHSON JUNCTION DEVICES AND DETECTORS BASED ON INCOHERENT COOPER PAIR TUNNELING**

**René Lindell**

Dissertation for the degree of Doctor of Science in Technology to be presented with due permission of the Department of Engineering Physics and Mathematics for public examination and debate in Auditorium F1 at Helsinki University of Technology (Espoo, Finland) on the 21<sup>st</sup> of October, 2005, at 12 o'clock noon.

**Helsinki University of Technology  
Department of Engineering Physics and Mathematics  
Low Temperature Laboratory**

**Teknillinen korkeakoulu  
Teknillisen fysiikan ja matematiikan osasto  
Kylmälaboratorio**

Distribution:  
Helsinki University of Technology  
Low Temperature Laboratory  
P.O. Box 2200  
FIN-02015 HUT  
Tel. +358-9-451-4909  
Fax. +358-9-451-2969  
E-mail: rene.lindell@iki.fi  
This dissertation can be read at <http://lib.hut.fi/Diss/>

© René Lindell

ISBN 951-22-7883-9  
ISBN 951-22-7884-7 (pdf)

Picaset Oy  
Espoo 2005



HELSINKI UNIVERSITY OF TECHNOLOGY P.O. BOX 1000, FI-02015 TKK <a href="http://www.tkk.fi">http://www.tkk.fi</a>		ABSTRACT OF DOCTORAL DISSERTATION	
Author			
Name of the dissertation			
Date of manuscript		Date of the dissertation	
Monograph		Article dissertation (summary + original articles)	
Department			
Laboratory			
Field of research			
Opponent(s)			
Supervisor (Instructor)			
Abstract			
Keywords			
Number of pages		ISBN (printed)	
ISBN (pdf)		ISBN (others)	
ISSN (printed)		ISSN (pdf)	
Publisher			
Print distribution			
The dissertation can be read at <a href="http://lib.tkk.fi/Diss/">http://lib.tkk.fi/Diss/</a>			



## Appended papers

This thesis is based on the following original publications.

- [P1] M. Sillanpää, T. Heikkilä, R. Lindell, and P. Hakonen, *Inverse proximity effect in superconductors near ferromagnetic material*, Europhysics Letters **56**, 590 (2001).
- [P2] R. Lindell, J. Penttilä, M. Paalanen and P. Hakonen, *Spectroscopy of mesoscopic Josephson junction using inelastic Cooper-pair tunneling*, Physica E **18**, 13 (2003).
- [P3] René Lindell, Jari Penttilä, Mika Sillanpää, and Pertti Hakonen, *Quantum states of a mesoscopic SQUID measured using a small Josephson junction*, Physical Review B **68**, 052506 (2003).
- [P4] R. Lindell, J. Delahaye, M. Sillanpää, M. Paalanen, E. Sonin and P. Hakonen, *Mesoscopic Josephson Junction as a Noise Detector*, Proc. of SPIE Vol. **5472**, 19 (2004).
- [P5] R. K. Lindell, J. Delahaye, M. A. Sillanpää, T. T. Heikkilä, E. B. Sonin, and P. J. Hakonen, *Observation of shot-noise-induced asymmetry in the Coulomb blockaded Josephson junction*, Physical Review Letters **93**, 197002 (2004).
- [P6] J. Delahaye, J. Hassel, R. Lindell, M. Sillanpää, M. Paalanen, H. Seppä, and P. Hakonen, *Low-Noise Current Amplifier Based on Mesoscopic Josephson Junction*, Science **299**, 1045 (2002).
- [P7] J. Delahaye, J. Hassel, R. Lindell, M. Sillanpää, M. Paalanen, H. Seppä and P. Hakonen, *Bloch oscillating transistor - a new mesoscopic amplifier*, Physica E **18**, 15 (2003).
- [P8] Rene Lindell and Pertti Hakonen, *Noise properties of the Bloch Oscillating Transistor*, Applied Physics Letters **86**, 173507 (2005).

- [P9] Rene Lindell and Pertti Hakonen, *Incoherent Cooper pair tunneling and energy band dynamics in small Josephson junctions: A study of the Bloch Oscillating Transistor*, REPORT TKK-KYL-016, May (2005).

## Author's contribution

The papers can be roughly divided into three subject areas where the author has been heavily involved in experiment and analysis: Application of  $P(E)$ -theory and small Josephson junctions in energy level spectroscopy ([P2], [P3]), noise spectroscopy with a Josephson junction ([P4], [P5]), and characterization and development of the Bloch oscillating transistor ([P8] and [P9]).

In publication [P1] the authors contribution was in writing the computer code and carrying out the numerical calculations based on  $P(E)$ -theory. The authors contribution to papers [P6] and [P7] was mainly of providing practical support at the different stages of the experiments involving sample manufacturing, cryogenics and measurement.

The authors largest contribution is in the experimental work in papers [P2], [P3], [P4], [P5], [P8] and [P9], which includes initial planning of the experiments, manufacturing the samples using electron beam lithography, managing cryogenics and carrying out the measurements and analysis of the measurement data using numerical calculations and simulations. Publications [P2], [P3], [P5], [P8] and [P9] were also for the most part written by the author.

# Contents

List of publications . . . . .	i
Author's contribution . . . . .	ii
<b>1 Introduction</b>	<b>1</b>
1.1 Organization of this thesis . . . . .	3
<b>2 Ultra Small Superconducting Tunnel Junctions</b>	<b>5</b>
2.1 Single electron tunnelling and Coulomb blockade . . . . .	5
2.2 Superconductivity and the Josephson effect . . . . .	6
2.3 RCSJ model of the Josephson junction . . . . .	7
2.4 Bloch states . . . . .	8
2.5 Environmental effects on Cooper-pair tunneling, $P(E)$ -theory	10
2.6 Extension of $P(E)$ -theory for non-Gaussian phase fluctuations	11
<b>3 Experimental techniques</b>	<b>15</b>
3.1 Electron Beam Lithography . . . . .	15
3.2 Measurement setup . . . . .	17
<b>4 Incoherent Cooper Pair Tunneling and Energy Spectroscopy</b>	<b>19</b>
4.1 Detection of energy levels in LC-oscillators . . . . .	19
4.2 Anharmonic correction . . . . .	22
4.3 Relaxation rates . . . . .	23
4.4 Evidence of Bloch energy bands . . . . .	25
<b>5 Noise spectroscopy</b>	<b>29</b>
5.1 Effects on Coulomb blockade due to non-Gaussian phase fluctuations . . . . .	29
5.2 Conductance versus noise current . . . . .	31
5.3 The ratchet effect . . . . .	34
<b>6 Bloch Oscillating Transistor</b>	<b>37</b>
6.1 Operating principle and simulation . . . . .	37

6.2	Measurement results . . . . .	39
6.2.1	Current and Power Gain . . . . .	39
6.2.2	Noise characteristics . . . . .	40
<b>7</b>	<b>Summary</b>	<b>45</b>
	<b>References</b>	<b>47</b>

# Chapter 1

## Introduction

THIS introduction strives to set the context in which this thesis work has been done and elaborate on some of the background and goals related to this field of research. The field of physics in which this thesis work was carried out is commonly known as nanophysics or mesoscopic physics. The former name gives a hint to what kind of length scales we are dealing with, or rather, what are the physical dimensions of the objects under study. The latter term, meso-, describes the field as studying phenomena happening in between the microscopic and the macroscopic worlds. The microscopic world is the world of atoms, where quantum mechanical laws must be used to describe the constitution of matter; the interaction between electrons, protons, photons and other elementary particles. The macroscopic world is the familiar world around us, where classical mechanics, based on Newton's laws of motion, are sufficient to describe most our daily observations. Mesoscopic physics is thus somewhere in the middle, where the structures can include millions of electrons, but where quantum mechanical effects can be observed in carefully designed experiments. The field thus strives to enlarge the structures where quantum mechanical effects can be observed and, eventually, to find novel high-tech, applications.

In mesoscopic physics the consequences of quantum mechanics — the wave nature of matter — become evident. Electrons cannot be considered as point like objects that interact simply like billiard balls. Their position, speed and their state cannot be deterministically obtained but only probabilities of their values can be given. Therefore, the quantum system stays in a linear superposition of many states, and the final state is resolved by a measurements process, where a macroscopic measurement apparatus is connected to the studied system. This peculiarity of quantum mechanics, the superposition of different states have been demonstrated also for macroscopically distinct states, such as currents flowing in opposite directions in a supercon-

ducting ring [1]. These findings are pushing the limits of our understanding and interpretation of quantum mechanics and nature [2]. How large can the "Schrödinger's Cat" be made? When does the final "collapse of the wave function" take place?

Another consequence of quantum mechanics is that electrically insulating barriers can be penetrated by electrons by leakage of their spatial probability mass, *i.e.*, their wave function, to the other side of the barrier, a phenomenon known as quantum mechanical tunneling. One of the main components of nanoelectronics - another name for this branch of mesoscopic physics - is the tunnel junction, which is formed by two conductors, often made out of aluminum, separated by a thin insulating oxide barrier. The tunnel junction has been proposed as a main building block for solid state quantum computers [3].

Nanoscale structures often restrict the physical space of the electrons to a small metallic island of the size of a few 100 nanometers, or roughly a thousandth part of the thickness of a human hair. The interaction of electrons due to Coulomb repulsion can make the current flow to the island quantized, which leads to the field of single electronics [4], where control of single electrons entering and leaving the island is achieved.

The concept of superconductivity adds an extra dimension to the field. By cooling down metals to very low temperatures, meaning 1.2 K or  $-272^{\circ}\text{C}$  in the case of aluminum, we find that the electrons condense into a new many-body state, called the superconducting state. In the superconducting state, the electrons are paired into so called Cooper pairs and the current can flow without resistance and metals act as perfect diamagnets. The superconducting state partly means that we can re-enter classical mechanics and the system can be described by a collective state of the electrons by two classical variables: an amplitude and a phase. However, these apparently classical variables, can at low enough temperatures also be shown to be quantum mechanical; a phenomenon sometimes called secondary quantum effect.

Superconductivity has already many practical applications, for example in the magnets of the levitating ultra fast trains and in the detection of very small magnetic fields, a technique called magnetoencephalography (MEG), used in studying the human brain. But, perhaps one of the most versatile structures that can be made out of superconductors is the superconducting tunnel junction, the so called Josephson junction [5]. This thesis deals mainly with studying the basic physics and the effect of the surrounding environment on the Josephson junction and the implications for Josephson devices. Taking into account the effect of the environment is a necessity as we can hardly ever isolate our studied system from the external surrounding. We need to know to what extent and how the surroundings affect the behavior of the studied

quantum system and, also, how we can control the environment to get well functioning quantum devices. The experimental realization of the Bloch oscillating transistor in Chapter 6 is an indication of what can be done with nanodevices when we have a good understanding of the underlying physics.

The main goal of physics research is to provide new scientific knowledge available to all mankind. Hence, when motivating the research in nanophysics, we should not only speak about applications and new devices, that lead to quick economic gains, but also be able to honestly declare that we are in the field of pure science, on a mission to understand nature and push the frontier of human knowledge. However, society as the main provider of funding for basic research, has a right to expect results, that hopefully will lead to economic growth and welfare. It is also a fact, that basic research does fuel innovations in the society and new surprising applications can be found, often only long after the main scientific work has been carried out. In this work, the main motivation has been scientific, although, it may happen that some of the measured devices or their improved versions could lead to applications in the future.

## 1.1 Organization of this thesis

This thesis is organized according to three related themes, which share a common theoretical background, based on phase fluctuation theory, briefly discussed in Chapter 2. The experimental methods involving fabrication of nanostructures and low noise measurement techniques at low temperatures are explained in Chapter 3. In the following chapters, the three themes are discussed: energy spectroscopy and observation of Bloch bands in Chapter 4, noise spectroscopy and non-Gaussian phase fluctuations in Chapter 5 and, finally, the Bloch Oscillating transistor in Chapter 6. The thesis is summarized in Chapter 7.



## Chapter 2

# Ultra Small Superconducting Tunnel Junctions

THE purpose of this chapter is to present a short introduction to the theoretical background most relevant for understanding the experimental results presented in the rest of this thesis. The experiments are presented in three Chapters as separate themes, but the theory in this Chapter is a unifying theme for all the observed phenomena. Therefore, the material presented below can be read as a framework needed for understanding the background and motivation for the experiments, at the same time showing how they beautifully can be described by the same language. Hence, it is logical that we start the discussion with the concept of Coulomb blockade and tunneling of normal electrons.

### 2.1 Single electron tunnelling and Coulomb blockade

One of the basic building blocks of mesoscopic physics is the tunnel junction, which consists of two conducting electrodes separated by a thin insulating barrier [6]. The normal tunnel junction, with either large dimensions, meaning large capacitance, or measured at large temperatures has a simple Ohmic  $IV$  curve, with resistance  $R_T$ . If the dimensions of the junction are made small enough we can see many additional, more interesting effects when the capacitive energy for single electrons plays a fundamental role [7]. The idea can be simply described as the fact that the addition of another electron to an isolated island, in its ground state, would require an amount of energy

equal to

$$E_C = \frac{e^2}{2C}, \quad (2.1)$$

where  $C$  is the electro-static capacitance of the island. In this manner, electrons can become localized in space and the current can be suppressed. The island can be constructed by a small quantum dot  $10 \text{ nm} \times 10 \text{ nm}$ , or a more extended island with a typical size of  $100 \text{ nm} \times 1000 \text{ nm}$ . The connection to the outer world is made by tunnel junctions, and the  $IV$ -curve over the whole system will have a threshold voltage  $V_C = E_C/e = e/2C$  before current starts to flow. The observation of the threshold voltage, known as the Coulomb blockade, requires that two basic requirements are met: 1) the temperature  $k_B T \ll E_C$ , and 2) the resistance seen by the junction  $R \gg R_K = h/e^2 = 25.8 \text{ k}\Omega$ . The more precise treatment of the effect of the electromagnetic environment on tunneling will be discussed in section 2.5. Typical experimental values for the capacitance of small tunnel junctions lie in the fF range, which means that the Coulomb energy corresponds to a temperature of 1 K and a threshold voltage of  $100 \mu\text{V}$ . Hence, the experiments have to be done at 100 mK or below, which requires the use of dilution refrigeration.

## 2.2 Superconductivity and the Josephson effect

The conducting parts of the nanocircuits used in this work were mostly made of aluminum, which turns superconducting at a critical temperature  $T_C = 1.2 \text{ K}$ . Therefore, from now on we mostly concentrate on the physics of superconducting tunnel junctions. Brian Josephson showed in 1962 [5] that in a tunnel junction made out of superconductors, a supercurrent can flow by tunnelling of Cooper pairs. From microscopic theory he derived the famous Josephson equations

$$\frac{d\varphi}{dt} = \frac{2eV}{\hbar} \quad (2.2)$$

$$I = I_C \sin \varphi, \quad (2.3)$$

that describe the time-evolution of the phase difference  $\varphi = \varphi_2 - \varphi_1$  between the superconductors on opposite sides of the junction. The supercurrent can have a maximum value up to the critical current  $I_C$  which can be calculated from the normal state tunnel resistance  $R_T$  using the Ambegaokar-Baratoff ( $T = 0$  assumed) relation [8]

$$I_C = \frac{\pi\Delta}{2eR_T}, \quad (2.4)$$

where  $\Delta$  is the superconducting gap, which is  $200 \mu\text{eV}$  for aluminum. However, in Section 2.5 the current through Josephson junctions will be shown to depend on the external environment.

An interesting fact that follows immediately from the basic Josephson relations is that the junction has an inductance  $L_J$ , which can be derived as follows. Taking the time derivative of Eq. (2.3) we get

$$\frac{dI}{dt} = I_C \cos \varphi \frac{d\varphi}{dt} = I_C \cos \varphi \frac{2eV}{\hbar} \quad (2.5)$$

$$V = \frac{\hbar}{2eI_C} \frac{1}{\cos \varphi} \frac{dI}{dt}. \quad (2.6)$$

Hence, the Josephson inductance is identified as

$$L_J(I) = \frac{\hbar}{2eI_C} \frac{1}{\cos[\arcsin(I/I_C)]} = \frac{\hbar}{2eI_C} \frac{1}{\sqrt{1 - \left(\frac{I}{I_C}\right)^2}} \quad (2.7)$$

The inductance thus depends on the biasing current  $I$ . For  $I \ll I_C$ , however, the inductance can be treated as a constant

$$L_J(0) = \frac{\hbar}{2eI_C}. \quad (2.8)$$

Together with the junction capacitance  $C$ , the Josephson junction forms an LC-oscillator with the resonance frequency

$$\omega_p = \frac{1}{\sqrt{L_J(0)C}} = \sqrt{\frac{2eI_C}{\hbar C}}, \quad (2.9)$$

which is also known as the plasma frequency (see Sec. 2.4).

## 2.3 RCSJ model of the Josephson junction

For many purposes, a good starting point for a more realistic description of the Josephson junction is the resistively and capacitively shunted junction model, familiarly known as the RCSJ model [8]. In this model an ideal Josephson junction is shunted by its own capacitance  $C$  and by some resistance  $R$ . The equation describing the current in this system is given by Kirchoff's law

$$I = C \frac{dV}{dt} + \frac{V}{R} + I_C \sin \varphi. \quad (2.10)$$

Using the Josephson relation (2.2) we can cast the equation into the form

$$I = \frac{\hbar C}{2e} \frac{d^2\varphi}{dt^2} + \frac{\hbar}{2eR} \frac{d\varphi}{dt} + I_C \sin \varphi. \quad (2.11)$$

An intuitive understanding of this equation can be found by the mechanical analogs of a forced pendulum with damping and a classical particle in a tilted washboard potential. This equation is commonly employed in describing the behavior of large Josephson junctions, where  $E_C \ll k_B T$ , and the phase can be treated as a classical variable.

The classical treatment also shows that if the washboard potential is high enough, and the temperature low enough so that we can ignore thermally activated jumps over barriers and quantum mechanical tunnelling through the barriers, the particle is localized at the bottom of one of the wells. Thus, the phase variable is constant, which means we have a supercurrent flowing through the junction in the manner of (2.3). The total current gives the tilt of the washboard potential, and if the tilt is large enough the particle can escape the well. In this case, a time averaged non-zero voltage develops over the junction and the system is in a dissipative mode.

## 2.4 Bloch states

It has been long known that the conjugate variable of the phase is the charge  $Q$  and that they satisfy the commutation relation [9]

$$[Q, \varphi] = 2ei. \quad (2.12)$$

This means, that the classical model of the previous section can be quantized, meaning that the phase  $\varphi$  is treated as a quantum mechanical variable [10]. This will then lead to new effects such as macroscopic quantum tunnelling of the phase and quantized energy levels within a well [10–14]. The situation when the particle is localized in one of the wells leads to a harmonic approximation when the well is deep enough (requiring  $E_J \gg E_C$ ), with the resulting energy levels

$$E_n = (n + \frac{1}{2})\hbar\omega_p, \quad (2.13)$$

where  $\omega_p$  is the plasma frequency of Eq. (2.9), which can be expressed as

$$\omega_p = \frac{\sqrt{8E_J E_C}}{\hbar}, \quad (2.14)$$

where we have introduced the Josephson coupling energy

$$E_J = \frac{\hbar I_C}{2e} \quad (2.15)$$

We will now jump to the full quantum mechanical picture and consider first the Hamiltonian of an isolated Josephson junction [15–17]

$$H = \frac{Q^2}{2C} - E_J \cos(\varphi) = -4E_C \frac{\partial^2}{\partial \varphi^2} - E_J \cos(\varphi), \quad (2.16)$$

$$4E_C \frac{\partial^2 \Psi(\varphi)}{\partial \varphi^2} + [E_J \cos(\varphi) + E] \Psi(\varphi) = 0. \quad (2.17)$$

The equation is known as the Mathieu equation, and it describes a particle in a periodic cosine-potential, with Bloch wave solutions  $\Psi_n^q(\varphi) = e^{i\varphi q/2e} u_n(\varphi)$ , where  $u_n(\varphi)$  is a  $2\pi$ -periodic function and the wave functions are indexed according to band number  $n$  and quasicharge  $q$ . The Bloch wave solution leads to a band structure of energy levels, similar to crystals in solid state physics [18] and, hence, the quasicharge  $q$  is analogous to the concept of crystal momentum. The instantaneous voltage over the junction is given by

$$V = \frac{dE_n(q)}{dq}, \quad (2.18)$$

and the real charge is thus  $\langle Q \rangle = C \langle V \rangle$ .

A more complete quantum mechanical description of the Josephson junction can be written as [16]

$$H = -E_C \frac{\partial^2}{\partial (\varphi/2)^2} - E_J \cos \varphi - \frac{\hbar}{2e} I \varphi + H_{env} + H_{int}, \quad (2.19)$$

where we now take into account the external bias current  $I$ , the Hamiltonian of the environment  $H_{env}$  and the interaction between the junction and the environment  $H_{int}$ . Considering first the effect of the external bias current  $I$ , at low temperatures and low current  $I \ll \delta E_1 e / \hbar$ , where  $\delta E_1$  is the first band gap, we find that the state of the system in  $q$ -space evolves adiabatically according to  $dq/dt = I$ . The system thus oscillates coherently in the first band, a phenomenon known as Bloch oscillation. At the quasicharge points  $q \pm e$ , Cooper pairs tunnel across the junction. The time averaged, DC voltage,  $\langle V \rangle$  is thus zero and this corresponds to the usual supercurrent state.

Due to the interaction term  $\propto I\varphi$ , the system can make transitions between energy bands via the so called Zener tunnelling [19,20]. The transition probabilities from band  $(n-1) \rightarrow n$  are given by the formula

$$P_{n,n-1}^Z = \exp\left(-\frac{\pi}{8} \frac{\delta E_n^2}{nE_C} \frac{e}{\hbar I}\right) = \exp(-I_Z/I), \quad (2.20)$$

where  $\delta E_n = E_n - E_{n-1}$  is the gap between bands  $n$  and  $n-1$  and,  $I_Z$  is the Zener break down current.

The system can relax from a higher to lower band by different mechanisms, due to fluctuations in the external environment or by tunnelling of quasiparticles.

## 2.5 Environmental effects on Cooper-pair tunneling, $P(E)$ -theory

The discussion so far has mainly concentrated on isolated Josephson junctions without any regard to the external environment. The electromagnetic environment, or the impedance, seen by the junction can be taken into account by different means. One relatively simple, perturbative approach, is the so called  $P(E)$ -theory [21–24], which starts from the Golden Rule for transition rates and takes into account the exchange of energy between the tunneling electrons, or in our case Cooper pairs, and the external environment. The basic results from the theory is that we need to know the  $P(E)$ -function, which describes the probability of energy exchange and which is given by the Fourier transform of the time averaged exponential phase-phase correlation function

$$P(E) = \frac{1}{2\pi\hbar} \int_{-\infty}^{\infty} dt e^{iEt} \langle e^{i\varphi(t_0)} e^{-i\varphi(t_0-t)} \rangle. \quad (2.21)$$

It can be shown that if the phase fluctuations of the environment are Gaussian, then the correlator above can be written as

$$\langle e^{i\varphi(t_0)} e^{-i\varphi(t_0-t)} \rangle = e^{J_0(t)}, \quad (2.22)$$

where  $J_0(t) = \langle [\varphi(t) - \varphi(0)]\varphi(0) \rangle$  is given by

$$J_0(t) = 2 \int_0^\infty \frac{d\omega}{\omega} \frac{\text{Re}(Z(\omega))}{R_Q} \{ \coth(\hbar\omega/(2k_B T)) [\cos(\omega t) - 1] - i \sin(\omega t) \}, \quad (2.23)$$

with  $R_Q = h/4e^2$ .

The  $IV$  curve is then given by [25]

$$I(V) = \frac{\pi e E_J^2}{\hbar} [P(2eV) - P(-2eV)]. \quad (2.24)$$

The  $IV$  is thus strongly dependent of the environmental impedance, a fact which formed the basic motivation for paper [P3].

## 2.6 Extension of $P(E)$ -theory for non-Gaussian phase fluctuations

The  $P(E)$ -theory discussed in the previous section was originally derived for Gaussian phase fluctuations, *i.e.*, for environments that can be defined by a classical impedance. Recently, the theory has been extended for the case where the phase fluctuations over the Josephson junction are non-Gaussian, which means that Eq. (2.22) can no longer be used [26].

If we assume that the equilibrium phase fluctuations from Gaussian sources are uncorrelated with the non-Gaussian ones we can write the general form of the Josephson junction current in the form [26]

$$I(V) = -\frac{2eE_J^2}{\hbar^2} \text{Im} \left\{ \int_0^\infty dt e^{J_0(t)} \left\langle \sin \left( \frac{2eVt}{\hbar} + \Delta\varphi_s \right) \right\rangle_{t_0} \right\}, \quad (2.25)$$

where  $\Delta\varphi_s = \varphi_s(t_0) - \varphi_s(t_0 - t)$  is the phase fluctuation due to the non-Gaussian sources and, the averaging  $\langle \dots \rangle$  is done with respect to all times  $t_0$ . Thus, the new problem will be to calculate the phase correlators  $\langle \cos \Delta\varphi_s \rangle$  and  $\langle \sin \Delta\varphi_s \rangle$ . When the extra noise source is that of quasiparticles from another tunnel junction, directly coupled to the island (the experiment to be discussed in Chapter 5), the phase fluctuations can be found by looking at the voltage fluctuations caused by the tunnelling quasiparticles

$$V_s(t) = \frac{I_S e}{|I_S| C} \sum_i \Theta(t - t_i) e^{-(t-t_i)/\tau}, \quad (2.26)$$

where  $I_S$  is the current through the noise junction,  $\Theta$  is the Heaviside step function and  $\tau = RC$  is the time-constant for the decay of the charge through an external resistor. The sum goes over the tunnelling events at times  $t_i$ , and thus to complete the calculation, one would need to specify the statistics of the tunneling events. The voltage peaks can be turned into phase steps by using the Josephson relation (2.3) written as

$$\varphi_s(t) = \frac{2e}{\hbar} \int_{-\infty}^t V(t') dt'. \quad (2.27)$$

Hence, the phase will take the form

$$\varphi_s(t) = \frac{I_S \pi \rho}{|I_S|} \sum_i \Theta(t - t_i) [1 - e^{-(t-t_i)/\tau}], \quad (2.28)$$

where  $\rho = R/R_Q$ .

The most relevant results for the experiment to be considered in Chapter 5 are summarized below. To simplify matters, the statistics of the tunneling process and the interaction between voltage pulses in Eq. (2.26) are ignored, meaning that pulses arrive at random but, well separated time intervals so that there is no overlapping of pulses. Following Ref. [26] we expand the  $IV$  curve as

$$I(V) = I_0 + GV + aV^2 + [b_0(T) + b_1] V^3, \quad (2.29)$$

where

$$G = G_0 + G_S \quad (2.30)$$

and,

$$G_S = \frac{\pi^{5/2}}{32\sqrt{2\ln(\rho)}} \left(\frac{E_J}{E_C}\right)^2 \frac{e}{E_C} \rho^{3/2} |I_S|. \quad (2.31)$$

Hence,  $G_0$  is the part due to the ohmic dissipation and  $G_S$  is due to the noise current. The ratchet effect, *i.e.*, non-zero current at zero bias voltage, is given by  $I_0$

$$I_0 = \frac{\pi^2}{32} \left(\frac{E_J}{E_C}\right)^2 \rho I_S. \quad (2.32)$$

The other expansion coefficients are

$$a = \text{sign}(I_S) \frac{C}{2e} G_S, \quad (2.33)$$

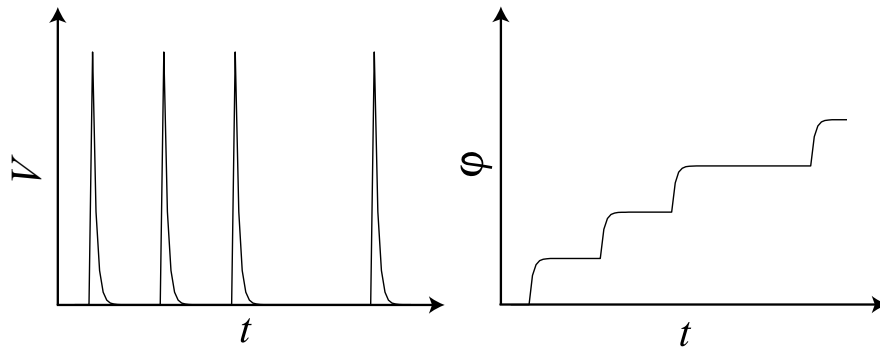


Figure 2.1: Illustration of the voltage peaks Eq. (2.26) and the corresponding phase steps Eq. (2.28), in arbitrary units.

$$b_1 = -\frac{\pi^2 C^2 \rho}{6e^2 \ln \rho} G_S, \quad (2.34)$$

whereas  $b_0(T)$  is a temperature dependent term due to Gaussian phase fluctuations in the Ohmic part of the environment.

From the expansion Eq. (2.29) we can derive the differential conductance

$$\frac{dI}{dV} = G + 2aV + 3[b_0(T) + b_1]V^2, \quad (2.35)$$

and, further, find an extremum of the conductance

$$V_{ext} = -\frac{a}{3[b_0(T) + b_1]}, \quad (2.36)$$

the nature of which is given by

$$\frac{d^2I}{d^2V} = 2a + 3[b_0(T) + b_1]. \quad (2.37)$$

Usually,  $|b_0(T)| - |b_1| > 0$ , for experimentally achievable temperatures  $\sim 50$  mK, and  $d^2I/d^2V > 0$ , thus making the extremum a conductance minimum. Thus, the non-Gaussian phase fluctuations should give rise to a shift of the minimum conductance according to Eq. (2.36).



## Chapter 3

# Experimental techniques

In this chapter, some of the experimental methods used to carry out the experiments are described. Firstly, the principles of sample manufacturing are laid out together with typical parameters used in the process. Secondly, the experimental setup and filtering at low temperatures is briefly discussed. In practice, the sample manufacturing stage can be a significant portion of the total experimental work. Therefore, it is relevant to discuss the different methods and resists used, and their relative merits.

### 3.1 Electron Beam Lithography

The fabrication method used for making the samples in this thesis was electron beam lithography and multiple-angle shadow evaporation [27], which have by now become standard in the field. The fabrication process can be divided into the following stages:

- Pattern design with 2D-CAD
- Preparation and spinning of oxidized silicon wafer with positive resist
- Patterning with JEOL JSM-6400 Scanning Electron Microscope (SEM) and Nanometer Pattern Generation System (NPGS) from JC Nability Lithography Systems
- Development of patterned chips
- Ultra High Vacuum (UHV) evaporation at  $10^{-9}$  mbar
- Lift-off

We will here concentrate on the choice of resist and its development procedures, which is one of the most crucial in the whole fabrication process (for more details, see *e.g.* Ref. [28]).

### PMMA/MAA

In the experiments described in Chapter 4, the resist employed in the sample fabrication was the commonly used PMMA and PMMA/MAA (polymethyl methacrylate/methacrylic acid) copolymer. The resists were prepared on a single crystal silicon wafer, with 300 nm thick SiO<sub>2</sub> insulating layer on top. The bottom PMMA/MAA copolymer layer was 480 nm thick and the top PMMA layer 80 nm. The structure was thus as shown in Fig. 3.1. After e-beam patterning at 20 kV acceleration voltage the samples were developed in MIBK (methyl-isobutyl-ketone):IPA (isopropanol) solution with 1:3 concentration and at 15° C. The samples were then rinsed in room temperature IPA and, occasionally, kept in ultrasonic bath for a few seconds. Since, the ultrasonic bath sometimes caused the collapse of the bridge structure for the small SQUID loops, the method was seldom used. The problem with the PMMA/MAA resist was that it was difficult to achieve enough undercut, especially, in the case of the Bloch Oscillating Transistor (BOT) samples. In the development phase, the IPA increases both the undercut and the upper window, which makes the separate control of the two layers difficult. However, by replacing the IPA with a solution of IPA:ethanol in 1:1 proportion, the development of the upper PMMA layer is slowed down while the bottom layer and undercut is still developed, thus more control can be achieved. With the PMMA/MAA structure, finding the correct dose for different structures can be time consuming, and it took several iterations of dose parameters to get sample yield up to about 50 %. The lift-off stage after the UHV evaporation, is quite straightforward with the PMMA/MAA. Putting the sample in acetone at 50° C, the lift-off could be readily done in 5 minutes.

### ZEP/PMGI-SF7

The BOT samples required more undercut than the previous samples, due to the four evaporation angles needed for making the structure. Therefore, we used another combination of resists: ZEP (= copolymer of -chloromethacrylate and -methylstyrene, which we mixed with Anisole in 1:2 volume proportion) from Nippon Zeon Corporation for the upper layer and PMGI-SF7 from Microchem for the bottom layer.

The development process for these resists was more difficult than for the PMMA/MAA. The upper ZEP layer is developed in n-amyl-acetate for

<b>PMMA 80 nm</b>	<b>ZEP 80 nm</b>
<b>PMMA/MAA 480 nm</b>	<b>PMGI 480nm</b>
<b>SiO<sub>2</sub> 300 nm</b>	<b>SiO<sub>2</sub> 300 nm</b>
<b>Silicon wafer</b>	<b>Silicon wafer</b>

Figure 3.1: Structure of the wafers with PMMA/MAA and ZEP/PMGI two-layer resists.

15-20 s, and rinsed in MIBK for 30-60s. At this stage, the result can be checked in an optical microscope, to see if the patterning was successful. Next, the bottom layer is developed in Microposit MF-322 developer (from Shipley) for 60s and rinsed in deionized water for 60s. Again, the result can be checked in optical microscope and the procedure with MF-322 & water is repeated until enough undercut is achieved. Also shorter development times, 30-45s, for the bottom layer were used if the sample received a larger dose during e-beam patterning. With this process one can separately control the upper and bottom layer development, a fact which made the bridge structure more stable and the sample yield could be improved as compared to the PMMA/MAA. Also, the dose can be kept constant at  $130 \mu\text{C}/\text{cm}^2$ , which simplifies the e-beam writing, but, at the same time requires that the SEM gives a stable low current of 1 – 4 pA, due to restrictions in the beam blanking time of JEOL 6400. Basically, all written and developed samples were good for evaporation making the sample yield at this stage close to 100 %.

The lift-off stage with the PMGI was done with Microposit 1165 remover (from Shipley). The 1165 was heated to about  $50^\circ \text{C}$  and the sample kept in the remover for 1-3 h. In the lift-off stage, many samples were ruined due to the fact that the PMGI was not completely removed all the way to the silicon wafer surface, and part of the metal structure came loose with the rest of the excess resist. Therefore, the development phase became crucial for this method and the cycling between MF-322 – water was always carried out a few times to make sure the PMGI was completely developed.

## 3.2 Measurement setup

The measurements system consisted of two dilution refrigerators: a plastic dilution refrigerator (PDR-50) from Nanoway (base temperature 34 mK) and another from Leiden Cryogenics (MNK-126-500) with a base temperature of

10 mK. The DC-wiring from room temperature to the sample holder consisted of superconducting twisted pair wires (Niomax). In the PDR-50, the wires were fed through 1 k $\Omega$  resistors situated at the 4.2K plate. The 1 k $\Omega$  resistors together with the line capacitance of  $\sim 1$  nF, act as RC-filters with cut-off at 10 MHz. On the sample holder there were 70 cm long Thermocoax cables for filtering high frequency, above 1 GHz, noise. The Leiden setup, besides having a 1 m long Thermocoax on the sample holder, had additional powder filters at mixing chamber temperature. Also, voltage division at mixing chamber temperatures was sometimes used with the Leiden setup, and this led to less noise and clearer observation of Coulomb blockade as compared with the PDR-50.

The low noise pre-amplifiers used in the experiments were the NF Instruments LI-75A voltage amplifier and Ithaco DL-1211 current amplifier. The LI-75A has a very low noise of  $\simeq 1.3$  nV/ $\sqrt{\text{Hz}}$  but it takes about 1h of stabilization before the amplifier stops drifting. The input DC- and AC-signals were generated with Hewlett Packard (HP/Agilent) 33120A signal generators and the amplified output fed to HP/Agilent 34401A multimeters for analog-digital conversion. AC-measurements were done with EG & G Instruments 7260 DSP lock-in amplifiers. For noise measurements we employed HP 89410A vector signal analyzer, which enabled the use of cross-correlation scheme [29], which involves calculating the correlation function

$$r_s(\tau) = E[v_1(t + \tau)v_2(t)], \quad (3.1)$$

between two signals  $v_1(t) = s(t) + w_1(t)$  and  $v_2(t) = s(t) + w_2(t)$  and taking their Fourier transform  $\mathcal{F}(r_s(\tau))$  that equals the power density. The two signals  $v_1(t)$  and  $v_2(t)$  are the outputs of two low noise amplifiers that both receive the same measurement signal  $s(t)$ . As the amplifier noises  $w_1(t)$  and  $w_2(t)$  are uncorrelated, the error of the signal power density goes down as

$$\sigma_s = s_n^2 \frac{1}{\sqrt{2 \cdot \text{RBW} \cdot T_m}}, \quad (3.2)$$

where  $s_n^2$  is the uncorrelated noise at the output of the amplifiers (voltage noise when employing voltage amplifiers), RBW is the resolution bandwidth ( $= f_s/N$ , *i.e.*, equal to the sampling frequency / averaging number) and  $T_m$  is the measurement time.

---

## Chapter 4

# Incoherent Cooper Pair Tunneling and Energy Spectroscopy

THIS chapter starts the review of the experiments done in this thesis. The first series of experiments were aimed at applying the ideas from  $P(E)$ -theory to see if small Josephson junctions can be used as classical inductive elements as in Section 2.2, or do they behave differently due to the interplay between the charging energy and the Josephson coupling energy in the manner of Sections 2.3 and 2.4. The experiments showed that we can go from the classical to the quantum regime by changing the ratio  $E_J/E_C$ . In the analysis of the experiments, the numerical methods used earlier for explaining the effect of inelastic tunneling in [P1] were further developed here and refined for fitting the measured data.

### 4.1 Detection of energy levels in LC-oscillators

The experimental idea is fairly simple: connect a Josephson junction, or rather, a SQUID, in series with a much smaller (about 10 times smaller in terms of junction area) Josephson junction and measure the  $IV$  characteristics of the smaller junction (this is similar to Ref. [30] where a classical transmission line was connected to a small Josephson junction). The use of a SQUID in this kind of experiment is natural, as in this way we can tune the ratio  $E_J/E_C$  by applying an external magnetic flux  $\Phi$  [31,32]. The Josephson energy of the SQUID then takes the form

$$E_J = \sqrt{E_J^1 + E_J^2 + 2E_J^1 E_J^2 \cos(2\pi\Phi/\Phi_0)}, \quad (4.1)$$

where  $E_J^1$  and  $E_J^2$  are the Josephson energies for the two junctions,  $\Phi$  is the externally applied magnetic flux perpendicular to the loop area and  $\Phi_0 =$

Sample # (component)	$R_T(k\Omega)$	$C$ (fF)	$E_J$	$E_C$	$E_J/E_C$
1 (Detector)	11.0	1.0	0.6	0.9	0.7
1 (2-SQUID)	1.4	9	5.3	0.1	53
2 (Detector)	166	0.5	3.6	160	0.023
2 (4-SQUID)	2.5	7.6	544 (272)	10.5	51.8
3 (Detector)	70	0.8	8.5	100	0.08
3 (1-SQUID)	3.5	5.7	422 (188)	14	30.1

Table 4.1: Sample parameters for the energy spectroscopy experiments. Each sample has a detector and an environment consisting of one or several SQUIDs. Homogenous or average parameter values are assumed for the SQUIDs. For samples 2 and 3, the value for  $E_J$  is that used in fitting the theory, while the Ambegaokar-Baratoff value is given in the parentheses. For more details, see the text. The energies are given in Kelvins.

$h/(2e)$  is the quantum of flux. In the case of a homogenous SQUID, where  $E_J^1 = E_J^2 = E_J^{single}$ , we get simply

$$E_J = 2E_J^{single} |\cos(\pi\Phi/\Phi_0)|, \quad (4.2)$$

and thus  $E_J$  can be tuned all the way to zero.

The ultra small Josephson junction, with dimensions of  $50 \times 50 \text{ nm}^2$ , will then act as the detector junction with an  $IV$  curve  $\propto P(2eV)$ , as described in the  $P(E)$ -theory of Section 2.5, Eq. (2.24). In simple terms, resonances, or transitions between energy levels in the detector environment will show up as peaks in the subgap  $IV$  curve at locations  $V_n = \Delta E_n/2e$  [33, 34].

In the first circuit design, we had four leads connected to the detector junction, two leads on each side, with a larger SQUID in each lead within a few  $\mu\text{m}$  of the detector (see Fig. 4.1) It is noteworthy that the closeness of the environment is important in all these experiments as the leads themselves constitute a capacitive coupling to ground, and the total capacitance increases with the length of the lead. Therefore, careful circuit design is necessary for a controlled electromagnetic environment.

With this 4-lead configuration, we could independently find all the parameters of the circuit. Furthermore, we could carry out 4-lead measurements and obtain the  $IV$  curve of the small detector junction. The first results led to three main observations:  $P(E)$ -theory with an  $RLC$  environment could be used to describe many of the observed  $IV$  curves satisfactorily, both qualitatively and quantitatively, but, there were discrepancies due to a larger array of peaks than what was expected and also the spacing of the observed peaks were not constant, as would be expected from a simple harmonic model.

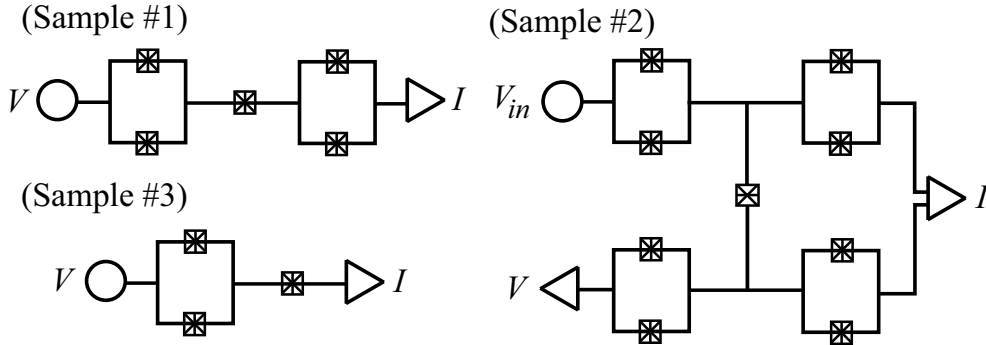


Figure 4.1: Circuit diagrams for the different samples (corresponding to Table 4.1) used in the energy spectroscopy measurements.

Our numerical methods for calculating the  $P(E)$  function for arbitrary impedances were based on the integral equation method of Ref. [35].

Some early results of a measurement involving a circuit with two leads connected to a detector junction (sample 1) with a single SQUID in each lead were published in article [P2]. In this experiment, the ratio  $E_J/E_C = 50$ , which meant that we were quite well in the classical regime and, therefore, the observed resonances followed quite closely the harmonic model. The interesting fact with this circuit was that the two SQUIDs had quite different parameters like the normal state resistance and capacitance. This meant that  $E_J/E_C$  could only be slightly tuned and, additionally, we found double the amount of resonances observed in the other experiments with more homogenous SQUIDs due to the fact that the plasma frequency  $\omega_p$  was slightly different for the two SQUIDs. In Fig. 4.2 this is seen in the structure of the peaks of the highest  $E_J/E_C$  curve and as a broadening of the peaks in lower curves. The critical current of the detector junction was, however, so large in this experiment that the total current flowing through the circuit was in the order of 10 nA. Such large currents means large heating, shot noise, and thus broad peaks and poor resolution. In Fig. 4.2, three  $IV$  curves for different  $E_J/E_C$  values for sample 1 are shown. The plasma energy (2.14) for the SQUIDs in this and later samples was  $200 \mu\text{eV}$ . The plasma energy was thus almost the same for all SQUIDs in different samples, indicating that the  $\text{AlO}_x$  layer was quite insensitive to the oxidization times in the evaporation stage of the sample fabrication. In the curve for maximum  $E_J/E_C$ , the peaks are broad due to the asymmetry of the two SQUIDs with regards to  $E_J$ . The two lowest curves show nice sequences of 6 resonances, indicating that up to 6 excitations to higher harmonic energy levels in the SQUIDs could be observed.

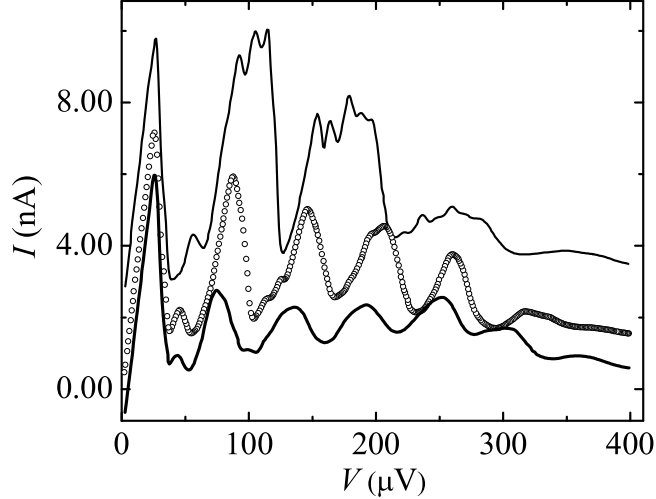


Figure 4.2:  $IV$  curves of sample 1, shifted in current for clarity: +2 nA for the highest curve and -1 nA for the lowest. The curves from top to bottom have the ratios  $E_J/E_C = 50, 29$  and  $21$ . In the top curve one can see the several resonances due to a slight difference in the plasma frequencies of the two SQUIDs

## 4.2 Anharmonic correction

The measurements of the 4-SQUID configuration presented in paper [P3] (sample 2) showed an improved resolution compared to the previous experiments (see Fig. 4.3). The most important reason for this was that the detector junction was much smaller, with a normal state tunnel resistance of  $R_T = 166$  k $\Omega$ , thus leading to currents of 10 – 100 pA, or 2-3 orders of magnitude smaller than in the experiment described in the previous section.

The improved resolution enabled more accurate comparison with theory. However, the  $P(E)$ -theory could only give a rough qualitative picture of the experiment. The  $IV$  corresponding to the maximum  $E_J/E_C$  ratio could be fitted fairly well with  $P(E)$ -theory, using an environment with 3 different  $RLC$ -resonators: one resonator represented all the four SQUIDs and its parameters could be determined from independent measurements, while the two other resonators were used to explain the non-flux dependent resonances (Fig. 4.3). The exact origin of the extra resonance peaks remained unknown but, as they varied from circuit to circuit, this indicated that they are spurious resonances generated by lead inductances and stray capacitances. The

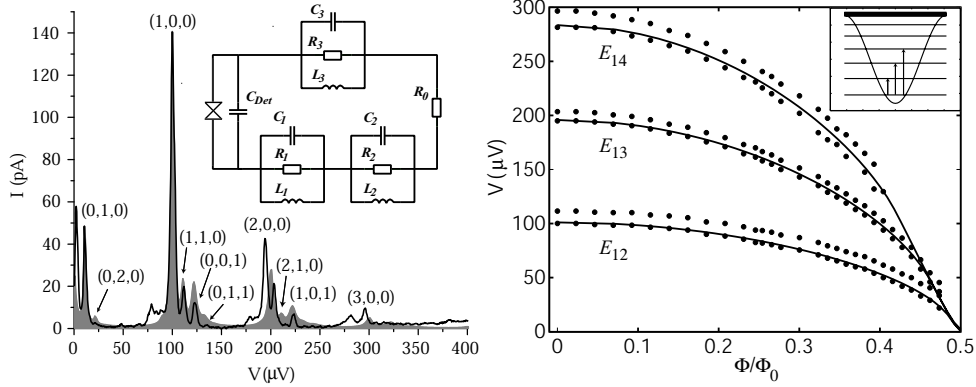


Figure 4.3: **(left)**  $IV$  curve of sample 2 and a fitted (shaded) curve of the 3- $RLC$ -resonator model shown in the figure. One resonator represents the four SQUIDS with equal parameters and two resonators are external, spurious line resonances. The excitations of each resonator is denoted by  $(n,k,l)$ . The parameters used in the simulation are  $C_{Det} = 0.5$  fF,  $C_1 = 4$  fF,  $L_1 = 2.28$  nH,  $R_1 = 50$  k $\Omega$  (SQUID),  $C_2 = 0.5$  pF,  $L_2 = 3.2$  nH,  $R_2 = 30$  k $\Omega$ ,  $C_3 = 2$  fF,  $L_3 = 10.8$  nH,  $R_3 = 3$  k $\Omega$ ,  $R_0 = 100$   $\Omega$  and  $T = 100$  mK. **(right)** Measured transitions and the theoretical lines calculated by numerically solving the Mathieu equation (2.17). The cosine potential and the transitions between the unequally spaced energy levels are shown in the inset.

experiment clearly revealed a multiphoton inelastic process, which had not been previously demonstrated. The process was that of exciting one mode in the SQUID and one in the extra resonance.

As mentioned earlier, the distance between the resonances were not constant. Therefore, the Schrödinger, or Mathieu equation of (2.17) was solved for the SQUID parameters in the experiment. In this way, the deviation from harmonic potential due to the shape of the cosine-potential was taken into account. There is a prominent double peak structure as clearly shown in Fig. 4.3. This feature is found in all samples and, has recently been explained by a quantum mechanical model, similar to the  $P(E)$ -theory, where resonators are coupled to two SQUIDS [36].

### 4.3 Relaxation rates

The results from the different circuit configurations, 2-lead vs. 4-lead measurements, differed mainly in the way the height of the peaks varied with the external flux. For the 2-lead measurements, the height quickly dropped as  $E_J$  was tuned down, as can be seen in the  $IV$  curves in Fig. 4.4. This fact

can be related to the sequential process of the current flow in the circuit: a Cooper-pair cannot tunnel in the detector unless it can excite the environment at energy  $\Delta E = 2eV$ , and this cannot happen before the environment has relaxed. Therefore, the current flow can be less than what is expected from the  $P(E)$ -theory, which always assumes that the environment has relaxed to the ground state before the next tunneling event. The relaxation process of the SQUIDs depends on the environment they see, *i.e.*, "the environment of the environment". By including the coupling term  $\propto i_n \varphi$  to include the effect of a noise current  $i_n$  as in Eq. (2.19), the down relaxation rate can be calculated using [37]

$$\Gamma_{\downarrow} = 2 \sum_{l < n} \text{Re}\{Y(E_{ln}/\hbar)\}(E_{ln}/\hbar)R_Q |\langle l|\varphi|n\rangle|^2, \quad (4.3)$$

where  $Y(\omega) = [1/(i\omega C_{det}) + R_0]^{-1}$  is the admittance seen by the SQUID and the last term is the matrix element of the transition from state  $n$  to state  $l$ . In Fig. 4.5, we show how the peak amplitude would be expected to go down as a function of  $E_J/E_C$  due to the environmentally induced relaxation rate and, compare this with the observed decrease in amplitude of the first resonance peak. The fit, with parameters  $R_0 = 65 \Omega$  and  $C = 0.8 \text{ fF}$ , clearly indicates that the observations favor the above interpretation.

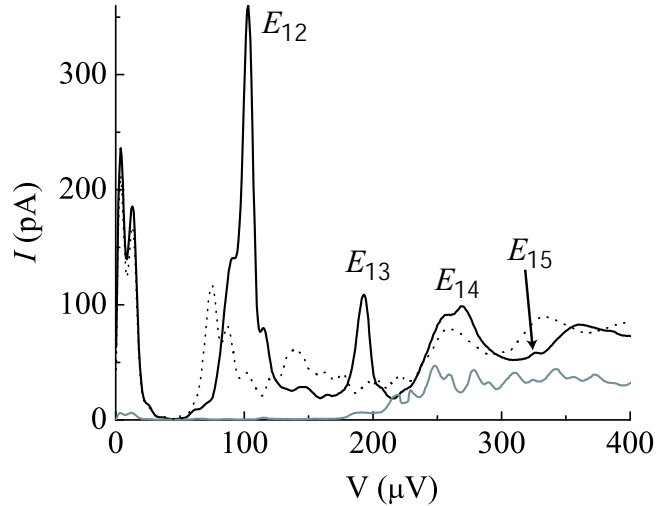


Figure 4.4:  $IV$  curves for sample 3 for fluxes  $\Phi/\Phi_0 = 0.0$  (highest curve),  $0.32$  (dotted line) and  $\simeq 0.5$  (lowest curve). The peaks indicated by  $E_{ij}$  correspond to the transitions between band edges shown in Fig. 4.6.

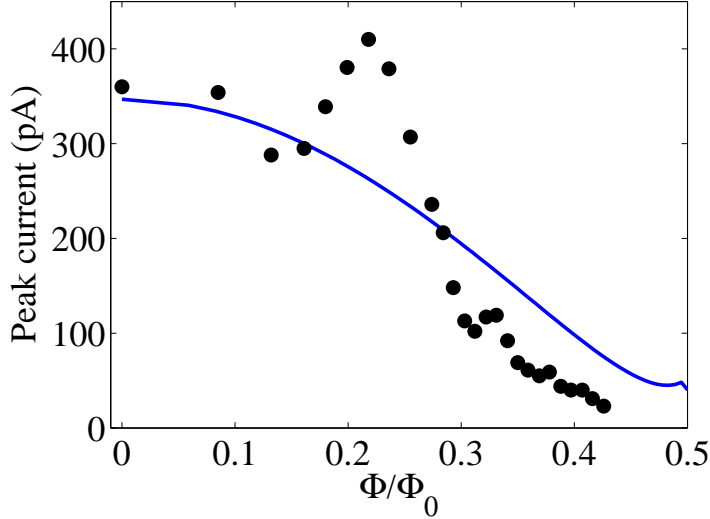


Figure 4.5: Amplitude of the first resonance peak of sample 3 ( $\bullet$ ) as a function of the external flux (see the peak movement in Fig. 4.4) and the theoretical line calculated with Eq. (4.3). The sudden increase in the peak amplitude is due to the fact that as the resonance frequency changes, it goes through an external resonance, which is independent of the applied flux. At this point the total tunneling current increases.

## 4.4 Evidence of Bloch energy bands

Finally, the experiments for low  $E_J/E_C$  values show that the peak structure strongly departs from the harmonic model and, in addition, that a simple fitting of discrete anharmonic states becomes impossible. The Mathieu equation of (2.17) allows a completely delocalized solution in phase space, resulting in the Coulomb blockade of Cooper pairs [38–42] and formation of energy bands [43–45]. In the experiment with one detector and one SQUID loop as the environment, we could observe evidence of the band structure in the splitting of the main resonance peaks (Fig. 4.6). The observations favors a model where we observe transitions between band edges. Thus, the band edges should be seen as Van Hove like singularities in density of states, or rather, in the occupation probabilities of the state. Processes that could generate this kind of peak in the probabilities includes the constant bias current  $q(t) = It$  and some mixing process which randomizes the charge states. As the DC-measurements are done fairly slowly, the randomizing process need not be fast in order for the outcome of the measurement be peaked at band edges. An alternative view [36] is that the band edges manifest themselves in

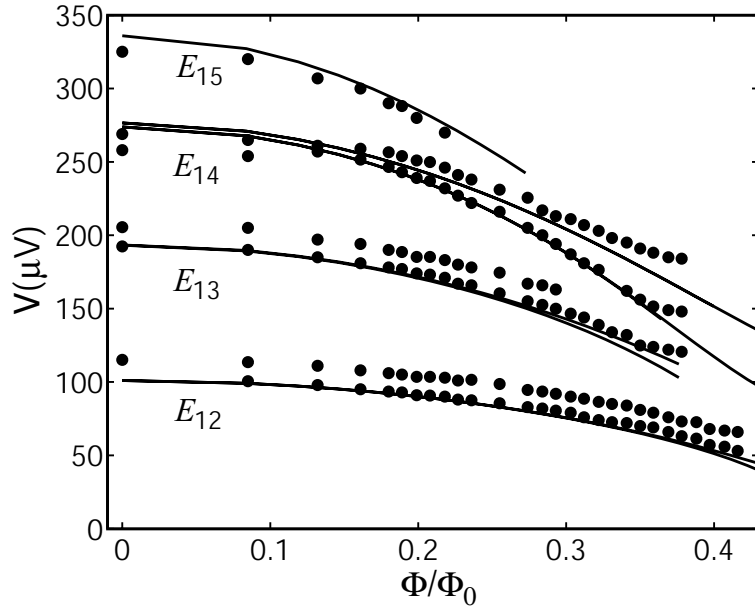


Figure 4.6: Location of the resonance peaks ( $\bullet$ ) as function of the external flux and the theoretical transitions between Bloch bands (solid lines). The ratio  $E_J/E_C$  thus goes from the maximum value 30 down to 9 (for  $\Phi/\Phi_0 = 0.4$ ). The transitions  $E_{ij}$  correspond to the peaks in Fig. 4.4.

the width of the resonance peaks, when a constant that accounts for spurious noise or relaxation is first subtracted off. In either case, the experiment gives a new kind of direct evidence for the existence of Bloch bands in a mesoscopic Josephson junction and with this method we could observe up to five bands, which is more than has been previously measured.

From theory [17], we know that in order for the delocalization of the phase to be possible, we need the proper environment and interaction: the terms  $H_{env}$  and  $H_{int}$  in Eq. (2.19). The problem has also been studied experimentally in order to find the phase diagram of the Josephson junction in terms of the ratio  $E_J/E_C$  and  $\rho = R/R_Q$  [46]. In simple terms, one can say that we need to suppress the dissipation of the environment,  $\propto 1/R$ , in order for the phase to be delocalized. Thus, to observe Bloch bands, the environmental impedance seen by the Josephson junction has to be  $\gg R_Q$ . In this experiment, the only large resistance seen by the SQUID is the detector junction itself. As the detector is practically Coulomb blockaded, the main dissipation mechanism is the quasiparticle channel of the detector.

The observation of the Bloch bands means that the charge is a good quantum number and that the state of the SQUID in charge space could be modified by an external gate voltage. In our circuits, we had a gate lead close

to the junction, but the peaks did not move as a function of gate voltage. This is most likely due to the fact that the bands are too narrow compared to the broadening of the peaks from outside noise, which masks out the gate dependence.

The observation of the Bloch nose in paper [P9] is another clear indication of the dynamics of Bloch bands. In the sample of that experiment, the environment resistance was  $179\text{ k}\Omega$ — much higher than in the previous measurements, thus indicating that we need a very high impedance environment to clearly observe Bloch oscillations [47–50].



## Chapter 5

# Noise spectroscopy

NOISE in mesoscopic systems has recently gained a lot of attention both from a theoretical [51, 52] and experimental viewpoint [53–56]. Traditionally, measurements have been focusing on the first moment, *i.e.*, on the average current and the differential resistance. However, additional information on the physical processes giving rise to current is contained in the higher moments of the current, for example in the variance (noise power) [57, 58]. If we study all the higher moments of current, we enter the field of full counting statistics – a well known concept in quantum optics [59], but which has only recently diffused into solid state physics as well [51, 52, 60]. The idea to utilize a Coulomb blockaded Josephson junction for noise spectroscopy was a natural evolution from the environmental measurements and energy spectroscopy done earlier. In fact, the phase fluctuation measurements is a kind of noise spectroscopy. The paper [P4] reviews some of the experimental results of using a mesoscopic Josephson junction as a detector of phase fluctuations.

### 5.1 Effects on Coulomb blockade due to non-Gaussian phase fluctuations

The fact that noise influences the Coulomb blockade of a Josephson junction is nothing new. In fact, the observation of the blockade requires careful filtering of external noise so that noise temperature of the residual noise is less or equal to the base temperature of the measurement, given by the mixing chamber temperature and the dissipation due to current in the circuit. However, that the statistics of noise or the asymmetry of phase fluctuations can be detected with a Josephson junction, has only recently been proposed [26, 61–63]. There are, however, only few direct experimental observations of

the higher moments of shot noise, *e.g.*, the third moment was measured with mixing and spectrum analyzer technique in Ref. [64].

In the experiment of [P5], the basic circuit layout was that of the Bloch oscillating transistor (to be discussed in Chapter 6) shown in Fig. 5.1. The source of the shot noise is a superconducting-insulator-normal tunnel junction and the environment of the Josephson junction contains a large, 179 k $\Omega$  resistor, in order to get a well defined high impedance environment – a requirement for obtaining a strong Coulomb blockade of Cooper pairs. The detection scheme used here is a direct coupling of the noise current to the circuit island. A suggestion to use a capacitive coupling of the noise source, in order to isolate the effect of the third moment was made in Ref. [65].

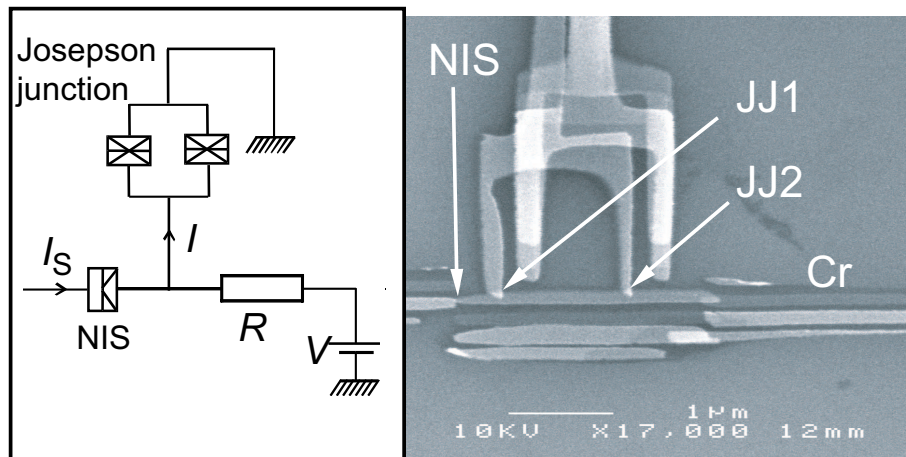


Figure 5.1: Circuit of the noise spectroscopy experiment and the scanning electron micrograph of a sample.

The main findings of how shot noise influences the Coulomb blockade can be summarized as:

1. The zero voltage conductance depends linearly on the shot noise current.
2. The ratchet effects appears as a consequence of the odd moments in the phase fluctuations.
3. The  $IV$  becomes increasingly asymmetric with a shift of the minimum conductance and the appearance of a local conductance maximum at non-zero voltages.

Pure shot noise can be characterized by its current power spectrum  $S_I = 2eI_S$ , which is a consequence of current fluctuations due to discrete charge carriers, in this case, tunneling electrons or quasiparticles. The statistics of the pure shot noise process is Poissonian. Hence, the probability distribution

	$R_T^{JJ} (k\Omega)$	$R_T^{NIS} (k\Omega)$	$R (k\Omega)$	$E_C$	$E_J^{min} / E_J^{max}$
1	8.1	27.3	22.6	65	22 / 78
2	24	73	179	80	2.4/24

Table 5.1: Sample parameters for two BOT samples used for noise spectroscopy.  $R_T^{JJ}$  is the normal state tunnel resistance of the Josephson junction and  $R_T^{NIS}$  is that of the NIS junction.  $R$  denotes the impedance of the Cr resistors in the immediate vicinity of the Josephson junction. The last two columns indicate the Coulomb energy,  $E_C$ , and the minimum  $E_J^{min}$  and maximum  $E_J^{max}$  values of the Josephson energy. The energies are given in  $\mu\text{eV}$ .

of the number of electrons that have tunneled during a time  $t$  is

$$P_t(n) = \left( \frac{I_S t}{e} \right)^n \frac{e^{-I_S t/e}}{n!} \quad (5.1)$$

In reality, the statistics of tunnel junction current is not always Poissonian but, depends on the environment of the junction and the interaction between the tunneling electrons. Hence, the actual noise power is commonly defined as  $S_I = F2eI_S$ , where  $F$  is the Fano factor.

## 5.2 Conductance versus noise current

In the experiment of [P5], the observations could for the most parts be explained with the extension of  $P(E)$ -theory as discussed in Section 2.6 and, especially, in Ref. [26]. The main observation was that the phase fluctuations created by tunneling quasiparticles in the NIS junction are non-Gaussian, and, therefore, have to taken into account in the theory. We here ignore Andreev reflection in the NIS interface (for noise in that case, see, *e.g.*, Ref. [66]) as it is not relevant for our experiment where we mostly bias above the quasiparticle threshold.

In Fig. 5.2, conductance curves for different values of the noise current are shown. The behavior reveals a large sensitivity for shot noise. Already a one pA change in the noise current gives a large change in conductance. The theory is strictly relevant for the zero bias case only, and it predicts the observed small shift of the minimum conductance. The competing shift is the trivial shift of  $RI_S$ , due to the fact that the noise current goes through the chromium resistor. When we subtract this trivial shift from the conductance curves, we get the results as shown in Fig 5.2, with the extrema located at constant points of voltage. As discussed in Section 2.6, the nature of the

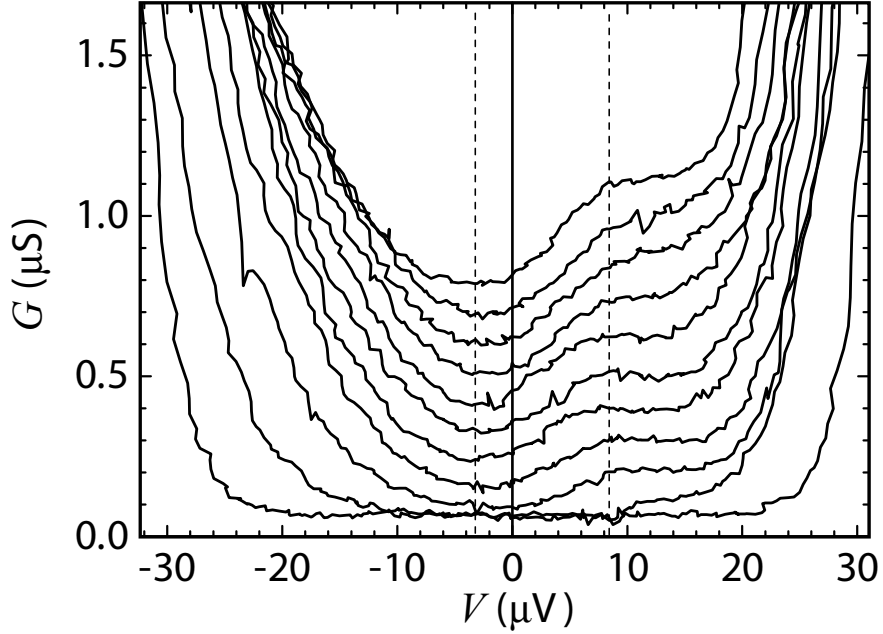


Figure 5.2: Differential conductance for the blockade region for sample 2 for noise currents 0-20 pA, with 2 pA steps per curve from bottom upwards. The voltage is measured across the Josephson junction and chromium resistor. The dashed lines indicate the locations of the conductance minimum and maximum.

extremum and the sign of the shift also depends on the effect of the underlying Gaussian noise generator in the resistor. However, from the experiment we find that the shift is  $-3.3 \mu\text{eV}$ . The observed sign of the shift means that the  $IV$  curvature due to the Gaussian noise source  $b_0(T) > 0$  dominates over the non-Gaussian noise  $b_1 < 0$  and leads to the observed negative sign in the shift Eq. (2.36).

Another effect of the shot noise is the appearance of a local conductance maximum. This can be thought of as due to raising of the time-averaged island voltage (2.26) due to the influence of tunneling quasiparticles. Numerical solution of Eq. (2.25) as well as numerical simulations in the manner of Chapter 6 also reveals a local conductance maximum, although the agreement with experiment is only qualitative.

In Fig. 5.3, the minimum conductance as function of the noise current is shown for different values of  $E_J/E_C$ . The dependence is linear after  $I_S \gtrsim 5$  pA when the effect of the noise current exceeds the background Gaussian noise generated by the chromium resistor. The experimental results are best compared with the theory from Sec. 2.6 by plotting the conductance mini-

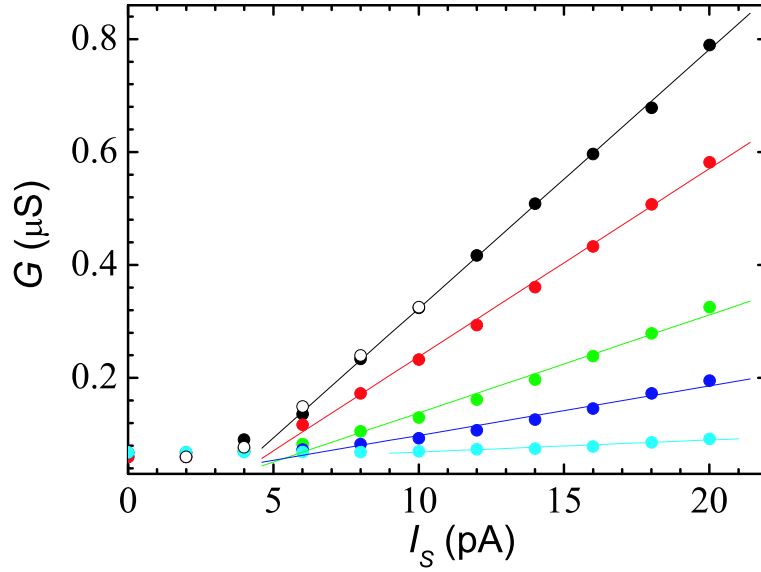


Figure 5.3: The conductance minimum as a function of  $I_S$  for  $E_J/E_C = 0.06, 0.11, 0.16, 0.24$  and  $0.3$  (from bottom upwards) for sample 2. The open circle data points are for the case of  $-I_S$ , thus showing that the effect is symmetric with respect to  $I_S$ .

mum as a function of the ratio  $E_J/E_C$  as is done in Fig. 5.4. The agreement with the theory is well within the experimental error margins of the parameters  $E_J$  and capacitance  $C$ .

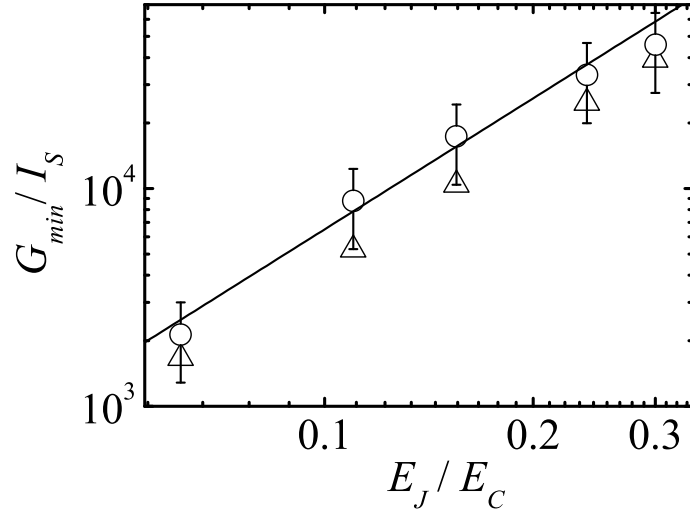


Figure 5.4: The slopes  $G_{min}/I_S$  of the linear part of the curves in Fig. 5.3 as a function of  $E_J/E_C$  for experimental ( $\circ$ ) and theoretical ( $\triangle$ ) data points calculated with Eq. (2.31). The line shows the fit of the power law  $\propto (E_J/E_C)^2$  to the experimental points.

### 5.3 The ratchet effect

The ratchet effect, which in our system is defined as the non-zero current for zero bias voltage, is another consequence of the asymmetry of the island phase fluctuations. The effect itself is an old concept in physics, especially in the well known problem of the ratchet and pawl (for an elementary discussion see, *e.g.*, Feynman Lectures on Physics Vol 1. Chapter 46 [67]), where the idea is to get work out of a heat bath at temperature  $T$  to another mechanical device at the same temperature by restricting the motion of a shaft by an asymmetric wheel, the ratchet and a pawl. The problem is clearly paradoxical as it seems to violate the second law of thermodynamics, but, by carefully studying the whole system, one can conclude that the device does not work unless there is a temperature gradient. The ratchet can, however, be shown to work for systems driven out of equilibrium by, *e.g.*, periodically turning on and off an asymmetric potential, which thereby supplies the required energy. Thus ratchet systems can be used as molecular motors in biology and particle filters or separators (for a thorough review on Brownian motors, see Ref. [68]).

In our sample #2, the ratchet effect is observed in the  $IV$  curves as a non-zero current for zero bias voltage (see Fig. 5.5). In Fig. 5.6, the size of the observed ratchet current is compared with the theoretically predicted  $E_J/E_C$  behavior of Eq. (2.32). The behavior is quite in accordance with the

theory of Ref. [26], which states that the ratchet effect is a manifestation of the odd moments of the phase fluctuations. The origin of the ratchet effect, in our system, can also be understood by the process where a quasiparticle tunneling to the island opens the Coulomb blockade of the Cooper pairs for the duration that it takes the quasiparticle to relax through the chromium resistor, thus allowing Cooper pairs to tunnel. The ratchet effect in our system could also be seen as a form of incoherent Cooper pair pumping [69].

All in all, one can say that the main experimental observations of the Josephson junction as detector of non-Gaussian noise are in line with the extended  $P(E)$ -theory discussed 2.6.

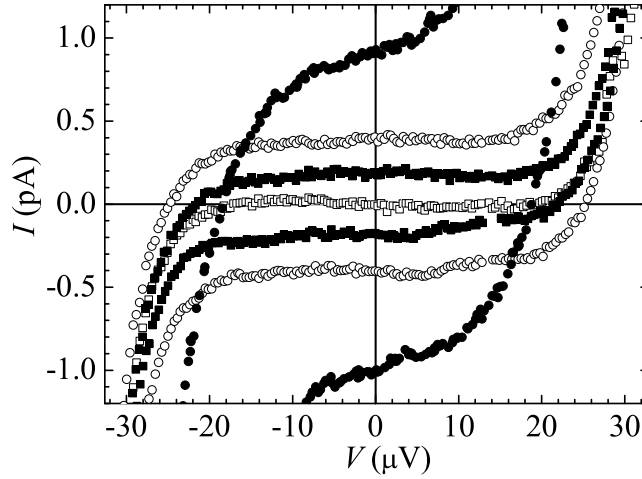


Figure 5.5: Coulomb blockade region  $IV$  curves for sample 2 for  $E_J/E_C = 0.3$ , showing the ratchet effect, *i.e.*, non-zero current for zero bias voltage due to the noise current  $I_S$ . The noise current goes through  $I_S = 0$  ( $\square$ ),  $\pm 0.2$  pA ( $\blacksquare$ ),  $\pm 0.4$  pA ( $\circ$ ) and  $\pm 2$  pA ( $\bullet$ ) from smallest to largest shift of  $IV$ .

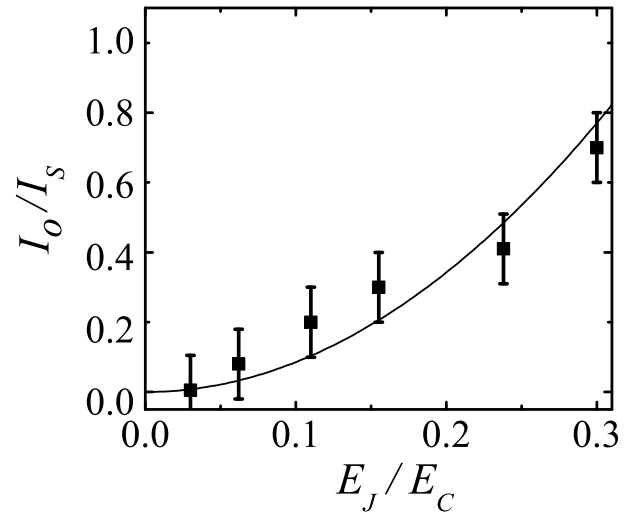


Figure 5.6: Ratchet current as function of  $E_J/E_C$  for sample 2. Solid line is the theoretical formula (2.32).

---

## Chapter 6

# Bloch Oscillating Transistor

THE Bloch Oscillating Transistor, or simply the BOT, is a new kind of mesoscopic device, which uses the quantum mechanical band structure of the Josephson junction and the Bloch oscillations therein as its main operating principle. The idea of the BOT was first suggested by Heikki Seppä at VTT (Valtion Teknillinen Tutkimuskeskus) and the simulations on the BOT was initiated by Juha Hassel [70–72]. The Low Temperature Laboratory became involved in the experimental realization of the BOT in 2002 and the work resulted in a demonstration of its operating principle in the article [P6].

### 6.1 Operating principle and simulation

The BOT is a three terminal device (see Fig. 6.2 below for the full measurement set-up and Fig. 5.1 for a SEM picture of the BOT) with the main components: a chromium resistor at the collector, Coulomb blockaded Josephson junction at the emitter, and a normal-insulator-superconducting (NIS) junction at the base. The principle of operation is based on the Bloch states theory of Section 2.4. The Coulomb blockaded Josephson junction, for which  $E_J \ll E_C$  and  $R \gg R_Q$ , can in the simplest case be described by two dynamical regimes, which also give rise to the model that explains the BOTs current amplification. The process of current amplification is illustrated in Fig. 6.1. In the Bloch oscillating regime, the JJ is in the lowest band and Cooper pairs are transferred coherently through the junction. In the Coulomb blockaded regime, the system has been excited by Zener tunnelling (2.20), or by environmental fluctuations, to a higher band and becomes blockaded, hence stopping the current flow. The relaxation to the ground state may happen through environmental fluctuations or by quasiparticle tunnelling. The role

of the base current is to control the down relaxation rate, so that a tunnelling quasiparticle through the NIS junction triggers  $\langle N \rangle$  Bloch oscillation cycles.

If we make the assumption that  $E_J \ll E_C$  so that the first two energy bands can be approximated by parabolas, the BOT operation can be predicted with Monte Carlo simulated by using the  $P(E)$ -theory (Sec. 2.5) for calculating both the inelastic Cooper pair tunnelling in the JJ as well as the quasiparticles rates in both junctions.

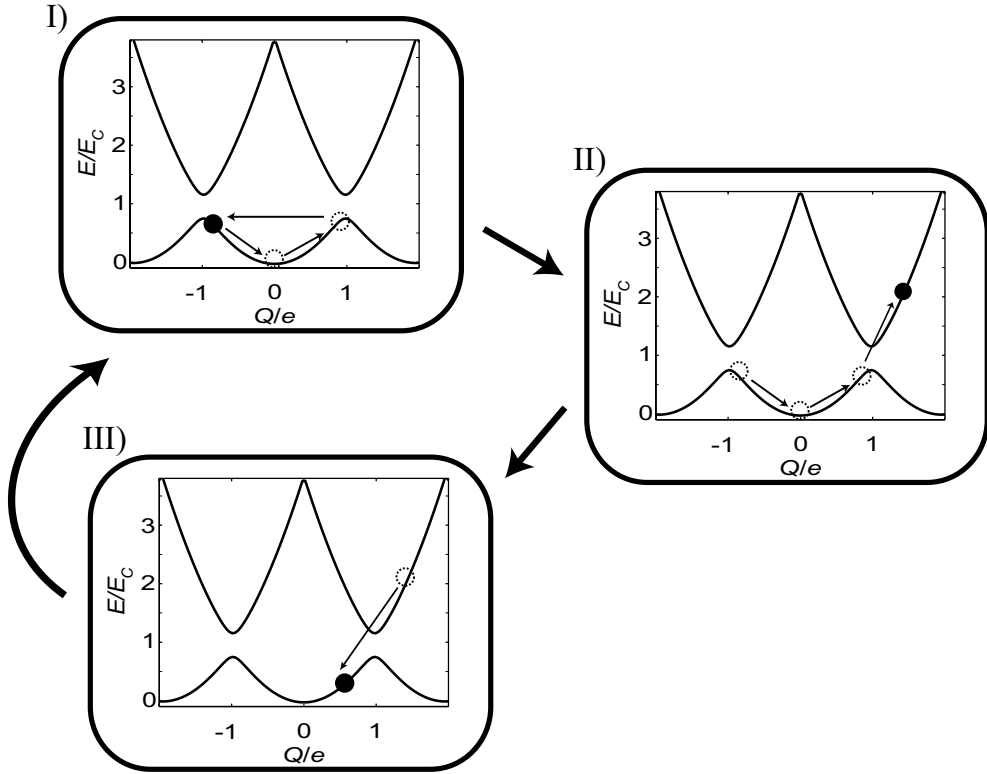


Figure 6.1: The principle of BOT operation as a current amplifier illustrated by energy band dynamics in the charge space. I) Bloch oscillations along the lowest band, with a Cooper pair tunnelling through the Josephson junction at the end of each period. II) Landau-Zener tunnelling to a higher band, making the JJ Coulomb blocked. III) Relaxation by quasiparticle injection through the NIS junction, thereby resuming the Bloch oscillations.

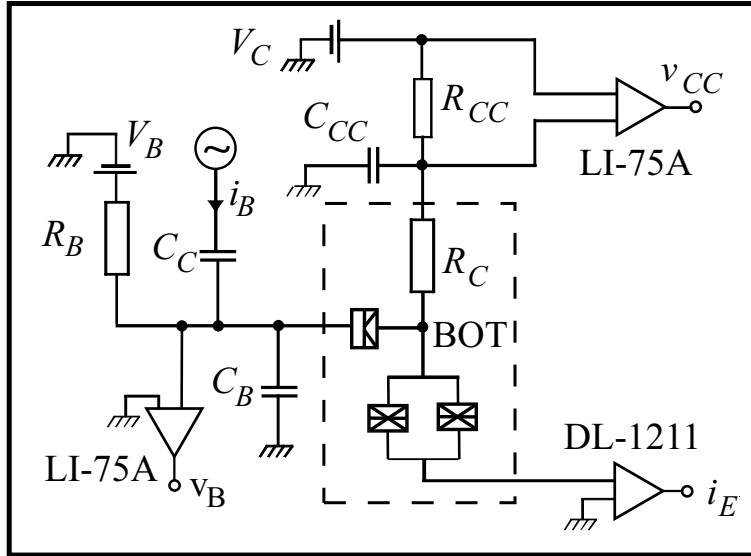


Figure 6.2: Scheme for power gain, current gain and input impedance measurements of BOT sample #2. The BOT circuit is bounded by the dashed box. The AC signal is capacitively coupled through the capacitor  $C_C$ . The signal from the pre-amplifiers LI-75A and DL-1211 are fed into lock-in amplifiers. The input current is fed through a large resistor  $R_B$  at room temperature. The capacitances  $C_B$  and  $C_{CC}$  are the capacitances from measurement leads and bond wires to ground. The resistor  $R_{CC}$  is a surface mount resistor, soldered to the sample holder.

## 6.2 Measurement results

### 6.2.1 Current and Power Gain

The first measurements which demonstrated that the BOT indeed operated as a current amplifier were reported in article [P6], which concerned the measurements on sample #1 (the sample parameters are given in Table 5.1). Another BOT with different parameters was then measured to gain further understanding on the power gain and noise properties. We start the discussion on BOT #2 by showing in Fig. 6.3 an  $IV$  with the corresponding current gain, calculated by direct subtraction of  $IV$ s taken with input currents of 400 – 410 pA. In this basic setup, the resistor  $R_{CC}$  was absent, meaning that the optimum operating region in terms of the input current is almost an order of magnitude larger (500 pA compared to 100 pA when  $R_{CC}$  was in place). Current gain as large as 35 was measured for this sample, which is also quite close to the value that was measured for sample #1.

The power gain was measured with the setup in Fig. 6.2, with the resistor

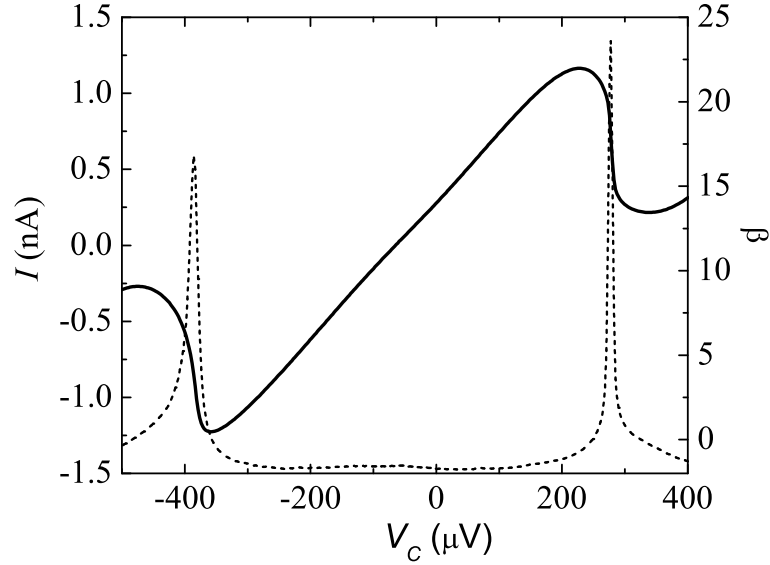


Figure 6.3:  $IV$  curve (solid line) and the current gain  $\beta$  (dashed line) for sample 2 with  $I_S = 400$  pA. Measurements were done without the resistor  $R_{CC}$ .

$R_{CC}$  acting as the load. In this way, we could define the power gain as

$$\eta = \frac{v_{CC}^2/R_{CC}}{i_B^2 Z_{in}}. \quad (6.1)$$

In Fig. 6.4 the power gain for BOT #2 is shown with a corresponding gain from simulation. The highest power gains measured were around 35.

## 6.2.2 Noise characteristics

The BOT noise characteristics are of great importance for evaluating the practical use of the device. The noise was measured with the setup shown in Fig 6.2. Here, the current noise at the collector was converted into voltage noise by the resistor  $R_{CC}$ . The signal was then amplified by the LI-75A and cross-correlated (explained in Section 3.2) in a HP 89410A vector signal analyzer. In this way, the voltage noise of the LIs were practically eliminated. The resulting measured output noise is then comprised of the noise due to the BOT itself, the residual current noise of the LIs and any spurious noise. We found that the residual noise, mainly due to the back-action of the LIs on the  $R_{CC}$  resistor, was  $2.6 \text{ nV}/\sqrt{\text{Hz}}$ . Therefore, to look at the input referred noise current we performed the transformation,

$$i_{nin}^2 = (i_{nout}^2 - i_{nres}^2)/\beta^2, \quad (6.2)$$

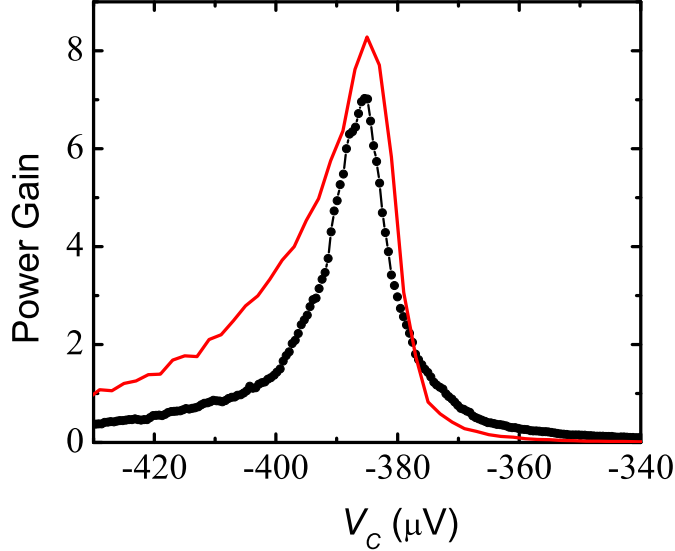


Figure 6.4: Power gain for  $I_S = 60$  pA in experiment ( $\bullet$ ) and simulation (solid line).

where the residual noise is subtracted from the output and, finally, the resulting noise is divided by the current gain at the operating point.

The main findings of the noise measurements are summarized in Figs. 6.5 and 6.6. The output current noise spectra density in Fig. 6.5 shows how the output noise does not grow linearly with increasing gain, as would be expected, but, seems to saturate to  $1/4$  of the input shot noise current. This means, that the input referred noise of Eq. (6.2) is actually decreasing and that correlations between output and input through the Coulomb blockade reduces the shot noise. Another way to think about the situation is to note that not every tunnelling quasiparticle in the NIS junction causes a downwards transition in the Josephson junction. Therefore, only part of the noise current is amplified.

The input referred noise temperature, presented in Fig. 6.5 is calculated with Eq. (6.2) and

$$T_n = \frac{i_{nin}^2 Z_{in}}{k_B}, \quad (6.3)$$

which differs by factor of  $1/2$  from the usual form due to the fact that the input current and voltage noise of the BOT are fully correlated and add in amplitude, not in power.

The reduction in noise temperature as function of current gain goes as  $\sim 1/\beta$ . The experimental exponent is  $-1.0 \pm 0.1$  and the simulated -1.2. The lowest measured noise temperature was 0.4 K at an optimum working point where the power gain was 30, however, in simulation the noise temperature goes as low as 100 mK.

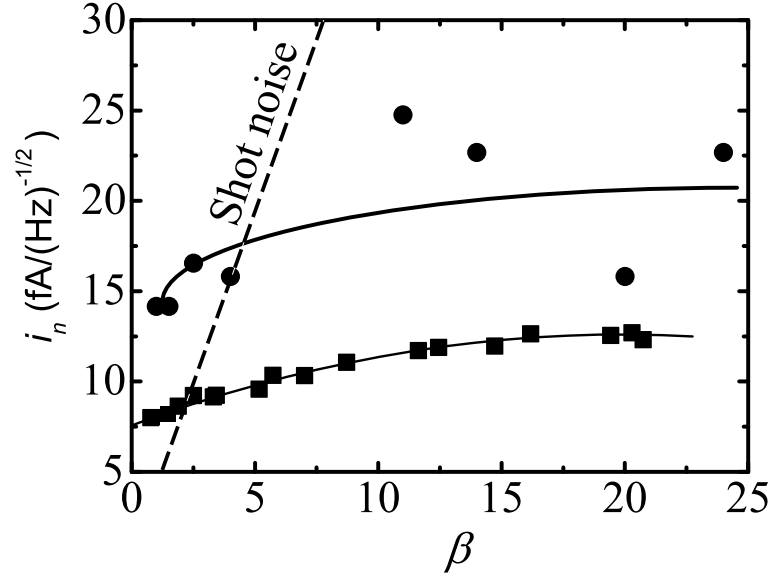


Figure 6.5: Output current noise spectral density as a function of current gain for BOT #2 in experiment ( $\bullet$ ) and simulation ( $\blacksquare$ ). The dashed line shows how the usual, constant shot noise current of the NIS junction  $I_{shot} = \sqrt{2eI_S}$  would, for a classical amplifier, be linearly amplified. The lines are to guide the eyes.

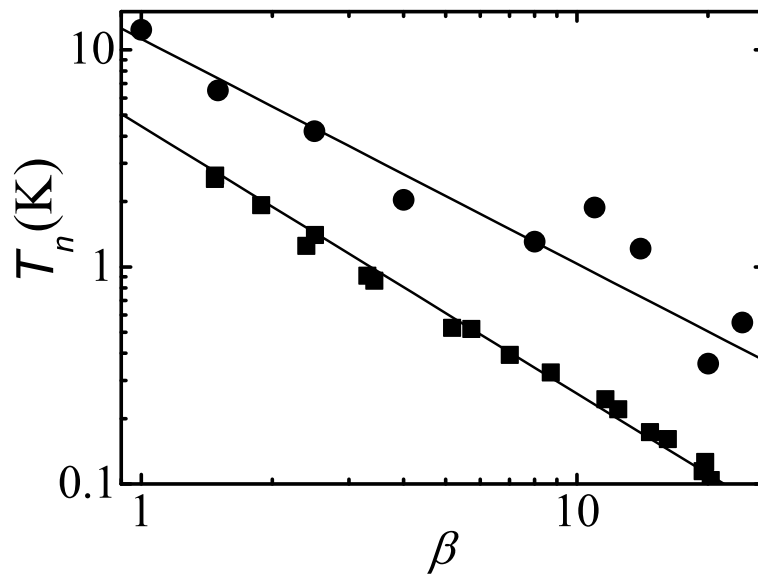


Figure 6.6: Noise temperature as a function of current gain for BOT #2 in experiment ( $\bullet$ ) and simulation ( $\blacksquare$ ).



# Chapter 7

## Summary

This thesis explored the effect of phase fluctuations on Cooper pair tunneling in a series of experiments which dealt with different aspects of the band dynamics and interplay between coherent and incoherent tunneling. The experiments found the mesoscopic Josephson junction to be a versatile device, which was used in studying the electromagnetic environment through energy spectroscopy, measuring asymmetric, non-Gaussian noise and using the band dynamics as a basis for realizing a mesoscopic amplifier.

The experiment on energy spectroscopy examined another method of probing the energy levels of the environment and, showed that a large Josephson junction behaves as an inductive environment, leading to equally spaced, harmonic oscillator-like energy levels, which, for smaller  $E_J/E_C$ , become increasingly anharmonic. When the Josephson energy was further reduced, the measurements also gave a new direct way of observing the band structure of the mesoscopic Josephson junction.

The Josephson junction was shown to be a sensitive device for measuring the character of external noise. In the detection of shot noise due to tunneling quasiparticles, the detector could react to noise currents well below 1 pA. The effects of an asymmetric noise source was observed in the shift of the minimum of the conductance curve and in the appearance of a local conductance maximum, as well as in the ratchet effect observed in the  $IV$  curves.

The Bloch oscillating transistor was extensively studied as a current and power amplifier, showing current and power gain larger than 30 and a measured noise temperature of 0.4 K. Still, there seems to be room for improvement on the theoretical side. A model, which self-consistently takes into account the interaction between the various components of the BOT circuit could be developed but, with the cost of increasing simulation time.

The future of Josephson junction devices in nanoelectronics is bright as

it has many possible applications, some of which have been presented in this thesis, and due to its proven robustness as the basic building block in quantum bit circuits [73, 74].

---

## References

- [1] J. R. Friedman *et al.*, Nature **406**, 43 (2000).
- [2] F. Laloë, Am. J. Phys. **69**, 655 (2001).
- [3] Y. Makhlin, G. Schön, and A. Shnirman, Rev. Mod. Phys. **73**, 357 (2001).
- [4] H. Koch and H. Lubbig, *Single-Electron Tunneling and Mesoscopic Devices* (Springer-Verlag, Berlin, 1992).
- [5] B. D. Josephson, Phys. Lett. **1**, 251 (1962).
- [6] T. A. Fulton and G. J. Dolan, Phys. Rev. Lett. **59**, 109 (1987).
- [7] D. V. Averin and K. K. Likharev, J. Low Temp. Phys. **62**, 345 (1986).
- [8] M. Tinkham, *Introduction to Superconductivity* (McGraw-Hill, New York, 1996).
- [9] P. W. Andersson, in *Lectures in the Many body Problem*, edited by E. Caianello (Academic, New York, 1964), p. 3.
- [10] J. Clarke *et al.*, Science **239**, 992 (1988).
- [11] J. M. Martinis, M. H. Devoret, and J. Clarke, Phys. Rev. B **35**, 4682 (1987).
- [12] P. Silvestrini, Y. N. Ovchinnikov, and R. Christiano, Phys. Rev. B **41**, 7341 (1990).
- [13] P. Silvestrini, V. G. Palmieri, B. Ruggiero, and M. Russo, Phys. Rev. Lett. **79**, 3046 (1997).
- [14] J. Claudon, F. Balestro, F. Hekking, and O. Buisson, Phys. Rev. Lett. **93**, 187003 (2004).
- [15] D. V. Averin, A. B. Zorin, and K. K. Likharev, Sov. Phys. JETP **61**, 407 (1985).
- [16] K. K. Likharev and A. B. Zorin, J. Low Temp. Phys. **59**, 347 (1985).

- 
- [17] G. Schön and A. D. Zaikin, Phys. Rep. **198**, 237 (1990).
- [18] C. Kittel, *Quantum Theory of Solids* (John Wiley & Sons, New York, 1963).
- [19] C. Zener, Proc. R. Soc. A **145**, 523 (1934).
- [20] E. Ben-Jacob, Y. Gefen, K. Mullen, and Z. Schuss, Phys. Rev. B **37**, 7400 (1988).
- [21] M. H. Devoret *et al.*, Phys. Rev. Lett. **64**, 1824 (1990).
- [22] G. Falci, V. Bubanja, and G. Schön, Z. Phys. B **85**, 451 (1991).
- [23] G.-L. Ingold and Y. V. Nazarov, in *Single Charge Tunneling*, edited by H. Grabert and M. H. Devoret (New York: Plenum Press, ADDRESS, 1992).
- [24] H. Grabert, G.-L. Ingold, and B. Paul, Europhys. Lett. **44**, 362 (1998).
- [25] D. V. Averin, Y. V. Nazarov, and A. A. Odintsov, Physica B **165** & **166**, 945 (1990).
- [26] E. B. Sonin, Phys. Rev. B. **70**, 140506(R) (2004).
- [27] G. J. Dolan, Appl. Phys. Lett. **31**, 337 (1977).
- [28] P. Rai-Choudhury, *SPIE Handbook of Microlithography, Micromachining and Microfabrication Volume 1: Microlithography* (SPIE, Washington, 1997).
- [29] M. Sampietro, L. Fasoli, and G. Ferrari, Rev. Sci. Instrum. **70**, 2520 (1999).
- [30] T. Holst, D. Esteve, C. Urbina, and M. H. Devoret, Phys. Rev. Lett. **73**, 3455 (1994).
- [31] Y. Harada and H. Takayanagi, Phys. Rev. B **54**, 6608 (1996).
- [32] M. Matters, W. J. Elion, and J. E. Mooij, Phys. Rev. Lett. **75**, 721 (1995).
- [33] A. D. Zaikin, J. Low Temp. Phys. **88**, 373 (1992).
- [34] G. Ingold, H. Grabert, and U. Eberhardt, Phys. Rev. B **50**, 395 (1994).
- [35] G.-L. Ingold and H. Grabert, Europhys. Lett. **14**, 371 (1991).
- [36] J. Leppäkangas, private communication (unpublished).
- [37] D. Esteve, M. H. Devoret, and J. M. Martinis, Phys. Rev. B **34**, 158 (1986).
- [38] D. B. Haviland *et al.*, Z. Physica B **85**, 339 (1991).
- [39] D. B. Haviland, L. S. Kuzmin, P. Delsing, and T. Claeson, Europhys. Lett. **16**, 103 (1991).

- 
- [40] L. S. Kuzmin and D. B. Haviland, Phys. Rev. Lett. **67**, 2890 (1991).
- [41] R. Yagi, S. Kobayashi, and Y. Ootuka, J. Phys. Soc. Jpn. **66**, 3722 (1997).
- [42] J. S. Penttilä *et al.*, Phys. Rev. Lett. **82**, 1004 (1999).
- [43] R. J. Prance, H. Prance, T. P. Spiller, and T. D. Clark, Phys. Lett. A **166**, 419 (1992).
- [44] H. Prance *et al.*, Phys. Lett. A **181**, 259 (1993).
- [45] D. J. Flees, S. Han, and J. E. Lukens, Phys. Rev. Lett. **78**, 4817 (1997).
- [46] J. Penttilä, Ph.D. thesis, Helsinki University of Technology, 2001.
- [47] L. S. Kuzmin, Y. Pashkin, A. Zorin, and T. Claeson, Physica B **203**, 376 (1994).
- [48] L. S. Kuzmin, Y. Pashkin, A. Zorin, and T. Claeson, Phys. Rev. B **54**, 10074 (1996).
- [49] M. Watanabe and D. B. Haviland, Phys. Rev. Lett. **86**, 5120 (2001).
- [50] M. Watanabe and D. B. Haviland, Phys. Rev. B **67**, 094505 (2003).
- [51] L. S. Levitov, H. Lee, and G. B. Lesovik, J. Math. Phys. **37**, 4845 (1996).
- [52] L. S. Levitov and M. Reznikov, Phys. Rev. B **70**, 115305 (2004).
- [53] A. Steinbach, J. M. Martinis, and M. H. Devoret, Phys. Rev. Lett. **76**, 3806 (1996).
- [54] R. J. Schoelkopf, A. A. Kozhevnikov, and D. E. Prober, Phys. Rev. Lett. **80**, 2437 (1998).
- [55] R. Deblock, E. Onac, L. Gurevich, and L. P. Kouwenhoven, Science **301**, 203 (2003).
- [56] J. Pekola *et al.*, cond-mat/0502446 (2005).
- [57] Y. M. Blanter and M. Büttiker, Phys. Rep. **336**, 1 (2000).
- [58] H. Grabert and G.-L. Ingold, Europhys. Lett. **58**, 429 (2002).
- [59] C. W. Gardiner and P. Zoller, *Quantum Noise* (Springer-Verlag, Berlin, 1996).
- [60] Y. V. Nazarov, Ann. Phys. (Leipzig) **8**, SI (1999).
- [61] C. W. J. Beenakker, M. Kindermann, and Y. V. Nazarov, Phys. Rev. Lett. **90**, 176802 (2003).

- 
- [62] J. P. Pekola, Phys. Rev. Lett. **93**, 206601 (2004).
- [63] J. Tobiska and Y. V. Nazarov, Phys. Rev. Lett. **93**, 106801 (2004).
- [64] B. Reulet, J. Senzier, and D. Prober, Phys. Rev. Lett. **91**, 196601 (2003).
- [65] T. T. Heikkilä, P. Virtanen, G. Johansson, and F. K. Wilhelm, Phys. Rev. Lett. **93**, 247005 (2004).
- [66] F. Pistolesi, G. Bignon, and F. Hekking, Phys. Rev. B **69**, 214518 (2004).
- [67] R. P. Feynman, R. B. Leighton, and M. Sands, *The Feynman Lectures on Physics* (Addison-Wesley, Reading, 1963).
- [68] P. Reimann, Phys. Rep. **361**, 57 (2002).
- [69] A. O. Niskanen, J. M. Kivioja, H. Seppä, and J. P. Pekola, Phys. Rev. B **71**, 012513 (2005).
- [70] J. Hassel, H. Seppä, J. Delahaye, and P. Hakonen, J. Appl. Phys. **95**, 8059 (2004).
- [71] J. Hassel and H. Seppä, cond-mat/0404544 (2005).
- [72] J. Hassel and H. Seppä, J. Appl. Phys. **97**, 023904 (2005).
- [73] D. Vion *et al.*, Science **296**, 886 (2002).
- [74] I. Chiorescu, Y. Nakamura, C. Harmans, and J. Mooij, Science **299**, 1869 (2003).